Two-dimensional oxygen-diffusion modelling for FLASH proton therapy with pencil beam scanning

Impact of diffusive tissue properties, dose, dose rate and scan patterns

Diepeveen, Maarten H.; Lathouwers, Danny; Santo, Rodrigo José; Hoogeman, Mischa S.; Habraken, Steven J.M.

DOI
10.1088/1361-6560/ad5eee

Publication date
2024

Document Version
Final published version

Published in
Physics in medicine and biology

Citation (APA)
Diepeveen, M. H., Lathouwers, D., Santo, R. J., Hoogeman, M. S., & Habraken, S. J. M. (2024). Two-dimensional oxygen-diffusion modelling for FLASH proton therapy with pencil beam scanning: Impact of diffusive tissue properties, dose, dose rate and scan patterns. *Physics in medicine and biology*, *69*(15), Article 155020. https://doi.org/10.1088/1361-6560/ad5eee

IOP Publishing Phys. Med. Biol. 69 (2024) 155020 https://doi.org/10.1088/1361-6560/ad5eee

Physics in Medicine & Biology

IPEM Institute of Physics and Engineering in Medicine

OPEN ACCESS

RECEIVED
22 December 2023

REVISED
26 May 2024

ACCEPTED FOR PUBLICATION
3 July 2024

PUBLISHED
24 July 2024

PAPER

Two-dimensional oxygen-diffusion modelling for FLASH proton therapy with pencil beam scanning—Impact of diffusive tissue properties, dose, dose rate and scan patterns

Maarten H Diepeveen[1,2], **Danny Lathouwers**[2,3,*], **Rodrigo José Santo**[1,3], **Mischa S Hoogeman**[1,2,3] **and Steven J M Habraken**[1,3,4]

[1] Erasmus MC Cancer Institute, University Medical Center Rotterdam, Department of Radiotherapy, Rotterdam, The Netherlands
[2] Delft University of Technology, Department of Radiation Science and Technology, Delft, The Netherlands
[3] Holland Proton Therapy Center, Department of Medical Physics and Informatics, Delft, The Netherlands
[4] Leiden University Medical Center, Department of Radiotherapy,Leiden, The Netherlands
[*] Author to whom any correspondence should be addressed.

E-mail: D.Lathouwers@tudelft.nl

Keywords: FLASH proton therapy, Proton therapy with pencil-beam scanning, Treatment delivery optimisation, Oxygen-diffusion modelling, Biological modelling

Abstract

Objective. Oxygen depletion is generally believed to play an important role in the FLASH effect—a differential reduction of the radiosensitivity of healthy tissues, relative to that of the tumour under ultra-high dose-rate (UHDR) irradiation conditions. In proton therapy (PT) with pencil-beam scanning (PBS), the deposition of dose, and, hence, the degree of (radiolytic) oxygen depletion varies both spatially and temporally. Therefore, the resulting oxygen concentration and the healthy-tissue sparing effect through radiation-induced hypoxia varies both spatially and temporally as well. *Approach.* We propose and numerically solve a physical oxygen diffusion model to study these effects and their dependence on tissue parameters and the scan pattern in pencil-beam delivery. Since current clinical FLASH PT (FLASH-PT) is based on 250 MeV shoot-through (transmission) beams, for which dose and dose rate (DR) hardly vary with depth compared to the variation transverse to the beam axis, we focus on the two-dimensional case. We numerically integrate the model to obtain the oxygen concentration in each voxel as a function of time and extract voxel-based and spatially and temporarily integrated metrics for oxygen (FLASH) enhanced dose. Furthermore, we evaluate the impact on oxygen enhancement of standard pencil-beam delivery patterns and patterns that were optimised on dose-rate. Our model can contribute to the identification of tissue properties and pencil-beam delivery parameters that are critical for FLASH-PT and it may be used for the optimisation of FLASH-PT treatment plans and their delivery. *Main results.* (i) the diffusive properties of oxygen are critical for the steady state concentration and therefore the FLASH effect, even more so in two dimensions when compared to one dimension. (ii) The FLASH effect through oxygen depletion depends primarily on dose and less on other parameters. (iii) At a fixed fraction dose there is a slight dependence on DR. (iv) Scan patterns optimised on DR slightly increase the oxygen induced FLASH effect. *Significance.* To our best knowledge, this is the first study assessing the impact of scan-pattern optimization (SPO) in FLASH-PT with PBS on a biological FLASH model. While the observed impact of SPO is relatively small, a larger effect is expected for larger target volumes. A better understanding of the FLASH effect and the role of oxygen (depletion) therein is essential for the further development of FLASH-PT with PBS, and SPO.

1. Introduction

In recent years, the FLASH effect has attracted a lot of attention in radiotherapy and particle therapy. It amounts to a differential reduction of the radiosensitivity of healthy tissue, relative to that of the tumour. While not all evidence has been conclusive, it has been repeatedly observed in animal experiments under ultra-high dose rate (UHDR, $>40-100\ \mathrm{Gy}\cdot\mathrm{s}^{-1}$) conditions, combined with moderate to high fraction doses (>3.5–10 Gy) (Puthenparampil Wilson *et al* 2012, Favaudon 2014, Vozenin *et al* 2019, Montay-Gruel 2021). The dependence of radiosensitivity on DR and the role of oxygenation therein have been studied extensively from the late 1950 s to 1970 s, e.g. Dewey and Boag (1959) reported an increase in damage of irradiation of bacteria in an oxygenated environment compared to hypoxic conditions. Later Hornsey and Alper (1966) and others obtained similar results on the dose-rate dependence of radiosensitivity in mice and mammalian cells (Town 1967, Berry *et al* 1969, Hornsey and Bewley 1971). The novelty of the paper by Favaudon (2014) from 2014 lies in the observation that the tumour is not spared under UHDR conditions. As such, FLASH as a differential effect amounts to a novel approach to further increase the therapeutic bandwidth of radiation therapy. An optimised FLASH effect could complement more well-established approaches such as fractionation and image-guided high-precision, highly conformal irradiation techniques.

The biological and physiological mechanisms behind the FLASH effect are not fully unraveled yet. Often discussed, mutually non-exclusive mechanisms that may play a role (Hughes and Parsons 2020) are (i) the reduced exposure and short irradiation and, hence, reduced radiation damage to circulating immune cells due to (ultra)short irradiation times, on the order of a few tens of milliseconds (Jin *et al* 2020, Almeida 2024), (ii) the reduction in radiation-induced reactive oxygen species (ROS) by an increase in simultaneously produced species, increasing inter-track interactions (Wardman 2020, Chappuis *et al* 2023), and (iii) the reduction in the generation of radiation-induced ROS which can damage DNA (Morgan and Sowa 2005, Zhu *et al* 2021) by the rapid radiolytic depletion of oxygen. UHDR pulses cause the depletion of oxygen due to radiation-induced chemical reactions (Spitz *et al* 2019). These chemical reactions occur faster than reoxygenation of the tissue and lead to hypoxic, more radioresistant conditions in healthy tissue compared to standard (normoxic) oxygenation conditions. Tumours are typically more hypoxic and therefore do not experience the sparing effect, or to a lesser extent. While changes in oxygenation and radiation-induced hypoxia through radiolytic oxygen depletion alone may not be sufficient to explain the observed magnitude of the FLASH effect[5], oxygen depletion is generally believed to play a role (Adrian *et al* 2020).

Most radiobiological FLASH experiments in animals have focused on UHDR 6-10 MeV electron beams (Montay-Gruel 2019, Vozenin *et al* 2019, 2022, Levy 2020). In 2019, the first patient was treated with an UHDR electron beam (Bourhis *et al* 2019). Pre-clinical studies also support evidence of the FLASH effect in cyclotron-accelerated therapeutic proton beams (van Marlen *et al* 2020). Recently, the first in-human clinical feasibility trial (FAST-01) on FLASH-proton therapy (FLASH-PT) of bone metastates in extremities has been completed (Mascia *et al* 2023). As opposed to UHDR MeV electron beams, FLASH-PT provides the possibility of irradiating deep-seated targets, while the physical properties of proton beams are superior to those of very high energy electron (VHEE) beams (Schüler *et al* 2017). With cyclotron-accelerated protons, the overall highest DR is achieved at the highest energy of (typically) 250 MeV. Current FLASH-PT is limited to such beams, which, in most clinical applications shoot through the patient (no Bragg peak inside the patient) and are referred to as transmission beams. Typically, the target is larger than the lateral extent of the beam, and the quasi-monoenergetic 250 MeV UHDR proton beam is combined with pencil beam scanning (PBS). This leads to complex spatiotemporal variations in dose delivery and local DR (Krieger *et al* 2022). To quantify the spatial variation in the local DR in UHDR-PT with PBS, Folkerts *et al* (2020) introduced a dedicated PBS-DR definition. José Santo *et al* (2022) showed that, for a fixed instantaneous DR and dose distribution, an optimised scan pattern may significantly increase the PBS-DR in stereotactic FLASH-PT of small lung lesions (Habraken *et al* 2022). Similar results were obtained by Deffet and Sterpin (2023). While the enhancement in PBS-DR is significant, it remains unclear what may be the impact of an optimised PBS-DR on the resulting FLASH effect.

In this paper, we address this issue by studying the impact of dose delivery and the spatiotemporal structure therein in a physical oxygen diffusion model, used here as a prototypical example of a radiobiological model that may describe the FLASH effect. To our best knowledge it is the first full two-dimensional oxygen diffusion model such that one can incorporate the impact of scan patterns (fully two-dimensional as in non-axially symmetric). Our model consists of regular network of capillaries through which the intermediate tissue is oxygenated. The oxygen tension within capillaries is fixed, thereby ignoring

[5] Experimental data on the FLASH effect in Favaudon (2014) is consistent with a FLASH-enhancement ratio of >1.8, which is substantially larger than typical oxygen enhancement ratios.

the transfer of oxygen by perfusion. The diffusion of oxygen through the tissue is modeled with a diffusion equation. Radiolytic oxygen depletion is taken into account through a dose-rate dependent oxygen loss term. The FLASH effect is described with a phenomenological model of oxygen-enhancement based on reference (Robert Grimes and Partridge 2015). With 250 MeV transmission beams and PBS, the spatiotemporal delivery dynamics close to the target varies primarily in the (x, y) plane transverse to the z axis along the beam. Since the beams travel through the patient, we limit ourselves to a two-dimensional model. As opposed to previous computational models by other groups (Robert Grimes and Partridge 2015, Pratx and Kapp 2019, Petersson *et al* 2020, Rothwell *et al* 2021, Hu *et al* 2022), which focused on the diffusion of oxygen through micro-meter scale networks of cells, our model is a physical model that captures the full range of length scales from the actual diffusion ($\sim$10 μm) to that of the capillary network ($\sim$ 100 μm) and that of the PBS delivery patterns ($\sim$6 cm). This allows the study of local as well as global FLASH effects and the effects of PBS on the oxygen induced FLASH effect.

This paper is organized as follows. In the next section, we present, discuss and discretise our model so as to numerically solve it. All relevant model parameters are identified and discussed, and a dimensional analysis is presented. After that, our results are presented in section 3 and discussed in section 4. A conclusion and outlook is presented in section 5.

2. Methods and materials

2.1. Oxygen diffusion model

We assume a regular two-dimensional network of capillaries through otherwise homogeneous tissue. Since we simulate transmission beams the dose deposition along the z-axis perpendicular to the two-dimensional plane in the patient is essentially constant. Limitations for diffusion in two dimensions when compared with three dimensions are considered in the Discussion. Oxygen is supplied through these capillaries are kept at a fixed oxygen tension, and diffuses through the tissue in between. The capillaries are configured on a regular rectangular grid on an area $A = 6 \times 6$ cm (see figure 1). This allows the study of a treatment plan for a patient with a stereotactic lung tumour with a gross tumour volume (GTV) of 7.5 mm and an area outside the GTV large enough so no FLASH effect is observed at the boundary of our area. Various patterns are used during irradiation to study the effect of the order of pencil beam delivery (see figure 2). The capillaries are separated in both dimensions by $d_x = d_y = 140$ μm. As a result, the largest distance between a capillary wall and a tissue voxel (pixel) is $d \approx 100$ μm (see illustration in figure 3), which is typically used as the largest distance from a capillary to tissue voxels (Secomb *et al* 1993).

Metabolic consumption, assumed constant and homogeneous throughout the tissue, and radiolytic depletion of oxygen are modeled with a loss term, leading to the following diffusion equation for the oxygen concentration

$$\frac{\partial C}{\partial t} = \nabla \cdot (\mathcal{D} \nabla C) - r \tag{1}$$

with C [mol $\cdot$ m^{-3}] the oxygen concentration, t [s] the time, $\mathcal{D}$ [m^2 $\cdot$ s^{-1}] the diffusion coefficient and r [mol $\cdot$ s^{-1} $\cdot$ m^{-3}] the oxygen loss term, discussed in more detail below. The following boundary conditions are imposed

$$\Gamma_n : \nabla C \cdot \hat{n} = 0 \,, \qquad \Gamma_b : C = C_{bc} \,, \tag{2}$$

the first one of which corresponds to a homogeneous Neumann boundary condition orthogonal ($\hat{n}$) to the outside boundary of the system (Γ_n). The second boundary condition imposes a fixed oxygen concentration C_{bc} on the boundary of a blood vessel (Γ_b), assuming a constant supply of oxygen from the capillaries. Both boundary conditions are illustrated in figure 1(a).

The depletion term r consists of two distinct contributions: (i) continuous and homogeneous metabolic consumption and (ii) radiolytic depletion, active during irradiation only. Metabolic consumption accounts for the continuous consumption of oxygen by cells and is approximated using Michaelis–Menten-style kinetics (Michaelis and Menten 2013) as given by

$$r_{\text{met}} = \frac{kC}{k_s + C}, \tag{3}$$

where r_{met} [mol $\cdot$ s^{-1} $\cdot$ m^{-3}] is the metabolic consumption rate, k [mol $\cdot$ s^{-1} $\cdot$ m^{-1}] is the maximum reaction rate and k_s [mol $\cdot$ m^{-3}] is the concentration at which the reaction saturates. Equation (3) approximates a constant consumption of oxygen when oxygen is abundant and smoothly tends to zero in its absence. Prior to taking into account the spatiotemporal dynamics of the delivery of radiation dose through a radiolytic

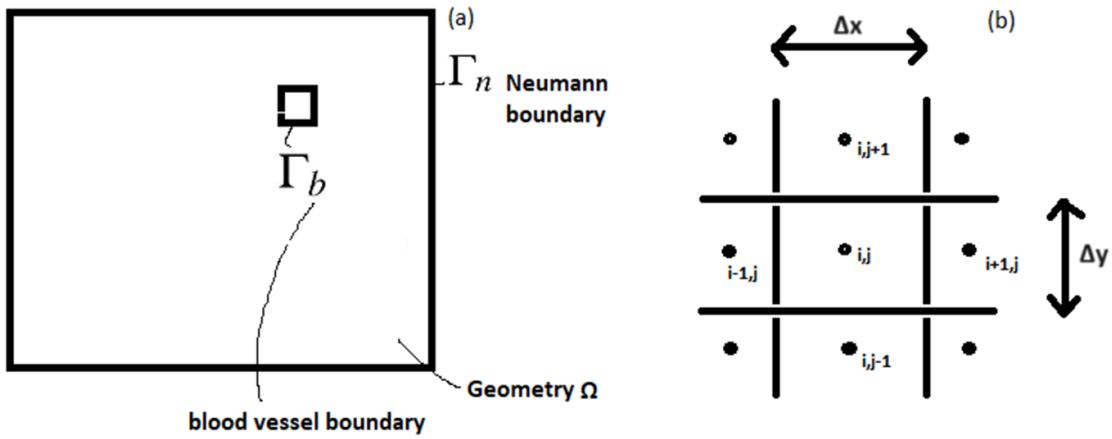

Figure 1. (a) The figure displays the finite 2D geometry Ω with an area $A = 6 \times 6$ cm^2 and the corresponding boundary conditions. Γ_n denotes the Neumann boundary condition on the border of the geometry. Γ_b denotes the boundary condition on the outside of a blood vessel, fixing the oxygen concentration. (b) The system is discretised in voxels where i denotes the horizontal location and j the vertical location of a voxel. The parameters Δx and Δy denote the horizontal and vertical separation respectively

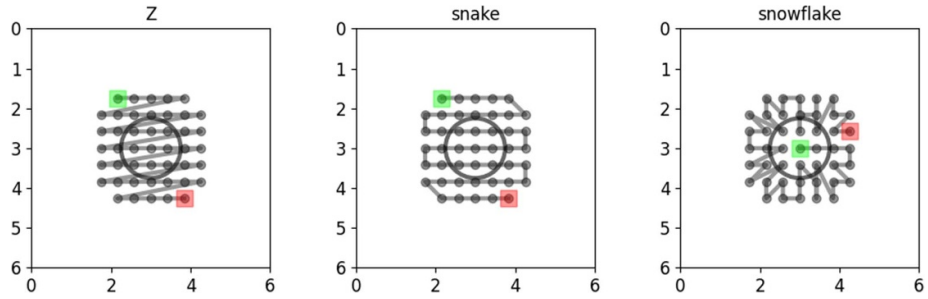

Figure 2. Various patterns which are used during irradiation, the pattern starts at the green square and ends at the red square. The black circle in the middle represents the tumour.

depletion term, equation (1) is numerically integrated to obtain the steady-state oxygen concentration for a given set of model parameters $\mathcal{D}$, r_{met} and C_{bc}.

While metabolic consumption (3) varies only through the spatially inhomogeneous variation in oxygen concentration, radiolytic depletion contributes only in voxels where dose is deposited during the delivery of a pencil beam. To model radiolytic depletion during irradiation, we assume a linear relation between (a constant and instantaneous) DR and the oxygen depletion rate

$$r_{\text{rad}} = k_d \dot{D}, \tag{4}$$

where r_{rad} [mol $\cdot$ s^{-1} $\cdot$ m^{-3}] is the radiolytic depletion rate, k_d [mol $\cdot$ m^{-3} $\cdot$ Gy^{-1}] is a proportionality constant and $\dot{D}$ [Gy $\cdot$ s^{-1}] is the (instantaneous) DR (Weiss *et al* 1974).

2.2. Discretisation and numerical integration

In figure 1(a), the finite 2D geometry Ω in which the model with appropriate boundary conditions will be solved, is displayed. In order to solve the diffusion equation (1), a finite volume method is applied. The equation is discretised in space on a two-dimensional voxel (pixel) grid with the volume of a voxel $V_{i,j} = \Delta x \cdot \Delta y$ (see figure 1(b)). Integrating equation (1) over a single voxel volume $V_{i,j}$, results in

$$\iint_{V_{i,j}} \frac{\partial C}{\partial t} \mathrm{d}x\mathrm{d}y = \iint_{V_{i,j}} \nabla \cdot (\mathcal{D}\nabla C)\, \mathrm{d}x\mathrm{d}y - \iint_{V_{i,j}} r\, \mathrm{d}x\mathrm{d}y\,. \tag{5}$$

Green's theorem is applied to the first term on the right-hand side resulting in

$$V_{i,j} \frac{\mathrm{d}C_{i,j}}{\mathrm{d}t} = \sum_f \int_{A_{f_{i,j}}} \mathcal{D}\nabla C \cdot \hat{n}\, \mathrm{d}A_f - V_{i,j} r_{i,j}\,, \tag{6}$$

where Σ_f denotes the sum over the four faces (sides) of a voxel (pixel) and A_f [m^2] denotes the area of the face of a voxel. The diffusive flux is then approximated using standard central differencing.

Assembling all unknowns $C_{i,j}$ in the vector $\bar{C}$, the system is written as

$$\bar{\bar{V}}\frac{\mathrm{d}\bar{C}}{\mathrm{d}t} + \bar{\bar{M}}\bar{C} = -\bar{\bar{V}}\bar{r}\,, \tag{7}$$

where $\bar{\bar{V}}$ is a diagonal matrix with the (equal) voxel volumes $V_{i,j}$ [m^2] on the diagonal, $\bar{C}$ [mol $\cdot$ m^{-3}] are the oxygen concentrations, t [s] is the time, and $\bar{\bar{M}}$ is the discrete Laplace operator.

To integrate over time, the Backward–Euler method is applied to equation (7), yielding

$$\bar{\bar{V}}\left(\frac{\bar{C}^{n+1} - \bar{C}^{n}}{\Delta t}\right) + \bar{\bar{M}}\bar{C}^{n+1} = -\bar{\bar{V}}\bar{r}^{n+1}\,, \tag{8}$$

where n denotes the step, Δt the discrete time step. Solving for $\bar{C}^{n+1}$ and grouping terms in front of $\bar{C}^{n+1}$ under $\bar{\bar{K}}_1$ and terms in front of $\bar{C}^{n}$ under $\bar{\bar{K}}_2$ results in

$$\bar{\bar{K}}_1\bar{C}^{n+1} = \bar{\bar{K}}_2\bar{C}^{n} - \bar{\bar{V}}\bar{r}^{n+1} \tag{9}$$

with $\bar{\bar{K}}_1$ and $\bar{\bar{K}}_2$ given by

$$\bar{\bar{K}}_1 = \frac{\bar{\bar{V}}}{\Delta t} + \bar{\bar{M}} \qquad \text{and} \qquad \bar{\bar{K}}_2 = \frac{\bar{\bar{V}}}{\Delta t}\,. \tag{10}$$

The discretised form of the metabolic consumption term is given by

$$r_{i,j\,\mathrm{met}} = \frac{k}{k_s + C^{n}_{i,j}}C^{n+1}_{i,j}\,, \tag{11}$$

while the discrete form of the radiolytic depletion is given by

$$r_{i,j\,\mathrm{rad}} = k_d\dot{D}_{i,j}\,. \tag{12}$$

Modelling radiolytic depletion with a term that is linear in DR may drive the oxygen concentration into negative values. To avoid such unphysical results, the radiolytic depletion is discretised as

$$r_{i,j\,\mathrm{rad}} = k_d\dot{D}\left(\frac{C^{n+1}_{i,j}}{C^{n}_{i,j}}\right)\,. \tag{13}$$

The full linear system is solved in each time step using a highly efficient multigrid solver (Germer *et al* 2020). All computations are performed on the Delft University of Technology supercomputer called DelftBlue (Delft High Performance Computing Centre 2022).

2.3. Dimensional analysis

In this paragraph, we perform a dimensional analysis of the model and the boundary conditions so as to identify a set of dimensionless parameters that fully characterise it. To this end, the diffusion equation with a loss term (1), boundary conditions (2) and depletion terms (3) and (4) are rewritten in terms of scaled dimensionless parameters

$$C' = \frac{C}{C_0}\,, \qquad t' = \frac{t}{t_0}\,, \qquad x' = \frac{x}{x_0}\,, \qquad y' = \frac{y}{y_0}\,, \tag{14}$$

where C_0, t_0, x_0 and y_0 are the scaling constants, which are arbitrary at this point. Substituting the dimensionless variables (14) in (1), and re-arranging the terms gives

$$\frac{\partial C'}{\partial t'} = \frac{\mathcal{D}t_0}{x_0y_0}\nabla' 2C' - \frac{\frac{kt_0}{C_0}C'}{\frac{k_s}{C_0} + C'} - \frac{k_d\dot{D}t_0}{C_0}\,, \tag{15}$$

such that the equation formally can be solved as

$$C' = C'\left(\frac{k_d\dot{D}t_0}{C_0}, \frac{k_s}{C_0}, \frac{kt_0}{C_0}, \frac{\mathcal{D}t_0}{x_0y_0}\right). \tag{16}$$

Table 1. table with the parameter values roughly based on the paper of Rothwell *et al* (2021), for a more exhaustive parameter and sensitivity analysis we refer to their paper.

Parameter	Parameter values
$\dot{D}$	$200, 400, 600\ \mathrm{Gy}\cdot\mathrm{s}^{-1}$
D	$18, 36, 54, 100$ Gy
$\mathcal{D}$	$[1.5, 1.75, 2, 2.5, 4]\cdot 10^{-9}\ \mathrm{m}^2\cdot\mathrm{s}^{-1}$
C_{bc}	40 mmHg
k	$0.01\ \mathrm{mol}\cdot\mathrm{s}^{-1}\cdot\mathrm{m}^{-3}$
k_s	$0.001\ \mathrm{mol}\cdot\mathrm{m}^{-3}$
k_d	$0.0005\ \mathrm{mol}\cdot\mathrm{m}^{-3}\cdot\mathrm{Gy}^{-1}$
A	$6x6\ \mathrm{cm}^2$
$d_{\mathrm{bloodvessel}}$	$10\ \mu$m
$\Delta x = \Delta y$	$5\ \mu$m
$\frac{\phi_O}{\phi_D}$	1.626
Ψ	$0.26\ \mathrm{mmHg}^{-1}$

where it is implicitly understood that C' also depends on the independent scaled variables x', y' and t'. The scaling constants (14) can be assigned any (dimensionfull) value relevant for the problem at hand. We choose $C_0 = C_{bc}$ where C_{bc} is the oxygen concentration on the capilary boundaries, $x_0 = y_0 = L$ where L is the distance between capillaries and $t_0 = D/\dot{D}$, such that the dimensionless parameters relate to (i) dose, (ii) irradiation time and (iii) diffusion. Substituting and re-arranging the dimensionless parameters results in

$$C' = C'\left(\frac{k_d D}{C_{bc}}, \frac{k_s}{C_{bc}}, \frac{C_{bc}\dot{D}}{kD}, \frac{C_{bc}\mathcal{D}}{L^2 k}\right). \tag{17}$$

In the calculations presented here, dose, DR and diffusion coefficient are varied. The second dimensionless parameter is a model constant. All parameter variations occur in the other three dimensionless parameters, which together fully specify the model parameter regime. This will be used to investigate in which parts of the model parameter space the (modelled) FLASH effect is most pronounced.

2.4. FLASH enhancement ratio

In general, the radiosensitivity of cells and tissues depends on the degree of oxygenation; under hypoxic conditions, cells and tissues are less sensitive to radiation damage than the same cells and tissues are under normoxic conditions. This difference in sensitivity is quantified by the oxygen enhancement ratio (OER), defined analogous to the relative biological effectiveness (Paganetti *et al* 2002) and commonly used in proton and heavy ion therapy. The OER is defined as the ratio of isoeffective dose levels under hypoxic and normoxic conditions at a fixed dose level and for a given (biological) end point, e.g. cell survival fraction in radiobiological experiments. The OER rate depends on cell/tissue type, on endpoint, on dose and on the oxygen concentration. In heavy particle therapy, it also depends on linear energy transfer (LET). Since we focus on the entrance part of proton transmission beams, the dependence of OER on LET can be neglected.

For our model, we follow the work of Robert Grimes and Partridge (2015), who established a relationship between the OER and the partial pressure of oxygen given by:

$$\mathrm{OER}\,(p) = 1 + \frac{\Phi_O}{\Phi_D}\left(1 - \mathrm{e}^{-\Psi p}\right), \tag{18}$$

where p [mmHg] is the partial oxygen pressure, Φ_O/Φ_D is the ratio of cells killed by oxygen fixation to the cells killed directly. The parameters Φ_O and Φ_D are the dose-dependent kill fractions. Their ratio is taken as a model parameter here, see table 1. Ψ is a parameter obtained by Robert Grimes and Partridge (2015) and also listed in table 1. The partial oxygen pressure can be related to the oxygen concentration through Henry's law, as given by Clark and Blanch (1997)

$$K_H^{pc} = \frac{p}{C}, \tag{19}$$

where K_H^{pc} is Henry's constant for which we use a value of $730\ \mathrm{mmHg}\cdot\mathrm{m}^3\cdot\mathrm{mol}^{-1}$ corresponding to the value for oxygen dissolved in water at 35° degrees.

Under the assumption that the FLASH effect solely depends on oxygen concentration, the OER can be inverted to give a FLASH enhancement ratio (FER). The FER is defined as the inverse of the OER,

normalised to the maximum OER as obtained from equation (18) in the limit of $\Psi p >> 1$, so

$$\mathrm{FER} = \frac{1 + \Phi_O/\Phi_D}{\mathrm{OER}}. \tag{20}$$

The FER is the reduction of biologically effective dose, due to the FLASH effect and results in no reduction under normoxic conditions at maximal oxygen enhancement and, for the model parameters used here (as listed in table 1), tends to a value of $1 + \Phi_O/\Phi_D = 2.626$ in fully hypoxic conditions. The effective dose, taking into account this FLASH effect, we refer to as FLASH-enhanced dose (FED). It is calculated for each voxel and in each timestep

$$\mathrm{FED}^n_{i,j} = \frac{D^n_{i,j}}{\mathrm{FER}^n_{i,j}}, \tag{21}$$

where the subscripts i, j denote a voxel and superscripts n denote a (discretised) time step. The total dose is divided by the total (time-integrated) FED to give the effective time-averaged $\overline{\mathrm{FER}}$ in each voxel, defined as

$$\overline{\mathrm{FER}}_{i,j} = \frac{D_{i,j}}{\sum_n \mathrm{FED}^n_{i,j}}. \tag{22}$$

The spatial distributions of the time-averaged $\overline{\mathrm{FER}}$ are used to study the effect of the diffusion coefficient, dose and DR and displayed in figures 5 and 6. The volume percentage of the PBS-DR and the FED for various parameter combinations is shown in figure 8. Furthermore, its dependence on the dimensionless parameters obtained above (17) is systematically assessed for a typical and realistic range of diffusive tissue and pencil-beam delivery parameters. The time-averaged $\overline{\mathrm{FER}}$ is averaged over the PTV (as defined below), resulting in a time-and space-averaged effective FLASH enhancement ratio

$$< \overline{\mathrm{FER}} >_{\mathrm{PTV}} = \frac{\sum_{i,j \in \mathrm{PTV}} \overline{\mathrm{FER}}_{i,j} \mathrm{d}V}{V_{\mathrm{PTV}}}, \tag{23}$$

where the brackets denote the averaging over space and dV is the volume of a voxel and V_{PTV} the volume of the PTV. The time-and space-averaged effective FER is used in a three-dimensional scatter plot and displayed in figure 9.

2.5. Treatment planning and modeling of treatment delivery

Analytically modeled pencil beams and treatment planning were used in this study. Planning was based on Gaussian pencil beams with a width of 3 mm (1 SD). The Gaussian distributions were normalised, so that the pencil-beam weights correspond to the integral dose per pencil beam.

A fixed region of interest of 6 cm × 6 cm was used. A circular GTV equal to the clinical target volume, with a radius of 7.5 mm (2.5 SD) at the centre of the region of interest was used. Since proton stopping power prediction errors do not play a role with transmission beam and assuming invariance of dose under shifts and local deformations, a PTV-based approach was used Habraken *et al* (2022). A fixed 7.5 mm (2.5 SD) margin was applied to obtain the planning target volume (PTV), which, as a result was also circular and had a radius of 15 mm (5 SD). Gaussian proton pencil beams were placed on a regular 4.2 mm square grid (1.4 SD, an integer multiple of $d_x = d_y$). Only pencil beams inside the PTV were included, see figure 2. The weights of the remaining pencil beams were optimised with a least-square optimisation to achieve a prescribed dose of 18 Gy, 36 Gy and 54 Gy inside the PTV, aiming at no dose outside of it. Fraction doses of 18 Gy (3 fractions) and around 34 Gy (single fraction) are commonly used in stereotactic treatment of early-stage lung cancer and lung metastases. For reference, also some simulations at a clinically unrealistic fraction dose of 100 Gy were performed for which we show the result in a volume histogram in figure 8(c).

The PBS-DR depends on the local spatiotemporal variation in dose delivery, and hence on the order in which the set of pencil beams comprising a treatment plan are delivered. This is referred to as a delivery scan pattern. For conventional treatments, standard back-and-forth line-by-line scanning ('snake' pattern) is used. In previous work by José Santo *et al*, we demonstrated that delivery scan patterns can be optimised with a genetic algorithm (José Santo *et al* 2022). Scan-pattern optimisation was performed sequentially so as to optimise the FLASH coverage at a fixed proton beam current, defined as the volume percentage that is irradiated during FLASH conditions ($D \geqslant 8$ Gy and PBS − DR $\geqslant 40$ Gy $\cdot$ s^{-1}). The resulting patterns minimise the time interval between the delivery of pencil-beam contributing dose to the same pixel/voxel, see figure 2, and are referred to as the 'snowflake' pattern (José Santo *et al* 2022). Here, we compare standard line-by-line scanning to the optimised patterns in terms of the resulting FLASH effect through radiolytic depletion of oxygen. Proton beam current was parameterised through the instantaneous integral DR of a pencil beam. Instantaneous integral DRs of 200 Gy $\cdot$ s^{-1}, 400 Gy $\cdot$ s^{-1} and 600 Gy $\cdot$ s^{-1} were used in this study.

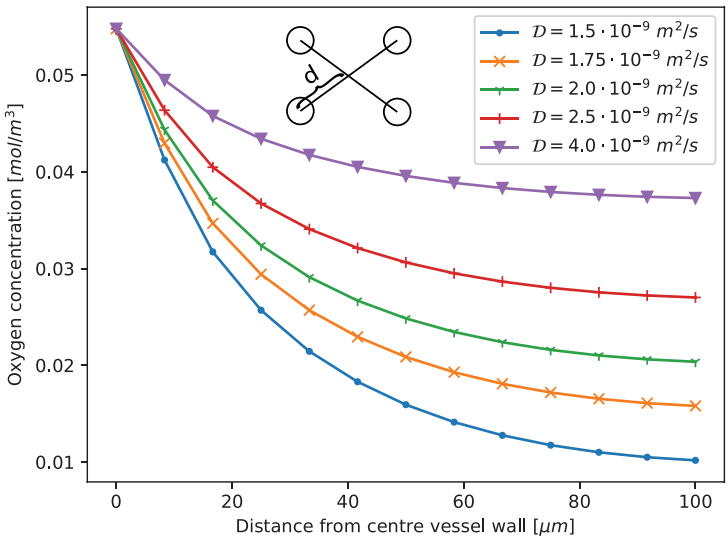

Figure 3. The steady-state oxygen concentration between diagonally opposite blood vessels for various diffusion coefficients. The two-dimensional geometry consists of blood vessels on a rectangular grid. The lowest oxygen concentration occurs at the largest distance ($d \approx 100\ \mu$m) from the blood vessel in the middle of the grid.

2.6. Model parameters, parameter uncertainties and model-parameter robustness

Values for the different parameters are listed in table 1. Different values of the diffusion coefficient, dose and DR are used to assess their impact on the steady-state oxygen concentration and the FLASH effect through its radiolytic depletion.

3. Results

3.1. Steady-state

Figure 3 displays the steady-state oxygen concentration for the various diffusion coefficients along the diagonal d. The resulting FLASH effect is largely dependent on the steady-state oxygen concentration and less on re-oxygenation, since oxygen depletion is orders of magnitude faster than re-oxygenation (Rothwell *et al* 2021). From equations (18) and (20) it can be derived that a significant FLASH effect may be achieved for $C \lesssim 0.014\ \text{mol} \cdot \text{m}^{-3}$. This implies that, for the lowest tested diffusion coefficient of $\mathcal{D} = 1.5 \cdot 10^{-9}\ \text{m}^2 \cdot \text{s}^{-1}$, a substantial portion of tissue is already in a hypoxic state in steady state, without any further radiolytic depletion of oxygen.

3.2. Dose distribution

Figure 4 displays the dose distribution for a dose of $D = 54$ Gy using the setup as described in the Methods and Materials, Treatment planning and modeling of treatment delivery. The treatment plan is optimised such that the combined contribution of the pencil-beams results in the minimal prescribed dose of in this case $D = 54$ Gy throughout the volume, with no dose outside the PTV. Therefore, at the locations of the pencil-beam the dose is larger. Since the dose distribution correlates linearly with the prescribed dose the figures for different doses are the same except for the colour bar, therefore, only the dose distribution of $D = 54$ Gy is presented.

3.3. Impact of the steady-state and the diffusion coefficient

Figures 5 and 6 display the $\overline{\text{FER}}$ distributions for various doses and DRs and a diffusion coefficient of $\mathcal{D} = 1.5 \cdot 10^{-9}\ \text{m}^2 \cdot \text{s}^{-1}$ and $\mathcal{D} = 2.0 \cdot 10^{-9}\ \text{m}^2 \cdot \text{s}^{-1}$ respectively. The diffusion coefficient is a critical parameter and has a large influence on the steady-state and the final resulting FLASH. Since it is uncertain what the actual oxygen concentrations are in tissue, and we observed that the computed oxygen induced FLASH effect for similar dose and DR is less than the FLASH effect observed in phenomenological experiments (Puthenparampil Wilson *et al* 2012, Favaudon 2014, Vozenin *et al* 2019, Montay-Gruel 2021). A more extensive analysis is performed on the diffusion coefficients of $\mathcal{D} = 1.5 \cdot 10^{-9}\ \text{m}^2 \cdot \text{s}^{-1}$ and $\mathcal{D} = 2.0 \cdot 10^{-9}\ \text{m}^2 \cdot \text{s}^{-1}$, where for larger diffusion coefficients the FLASH effect would reduce.

The vertical lines in figures 5 and 6 are due to the rectangular grid of capillaries, the oxygen distribution is symmetric with the overall lowest values achieved at the lighter blue vertical segments. For the lowest value

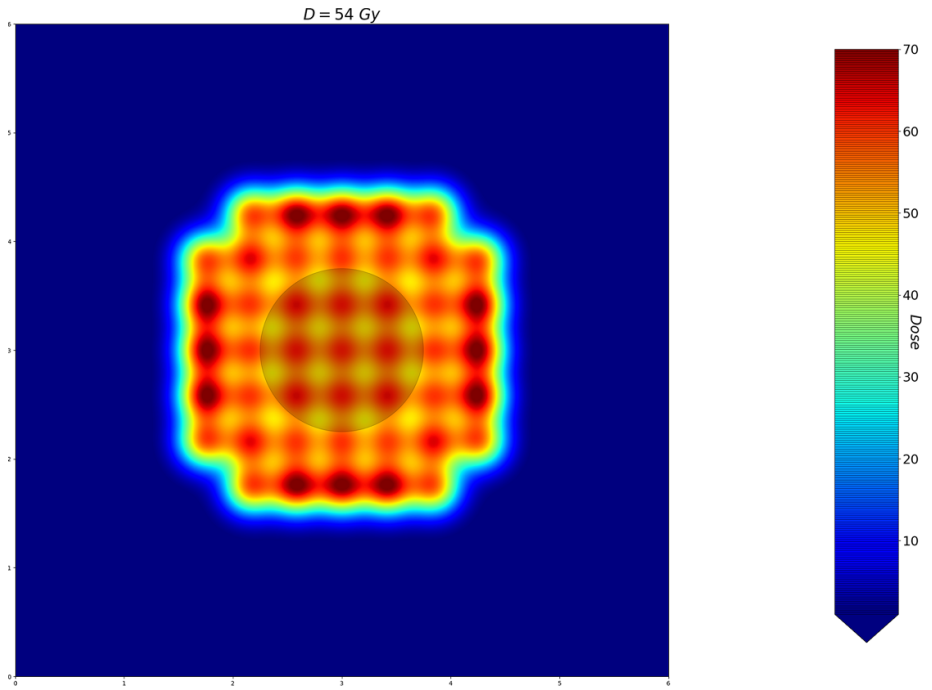

Figure 4. The dose distribution for a prescribed dose of $D = 54$ Gy. The opaque region in the middle of the PTV represents the tumour.

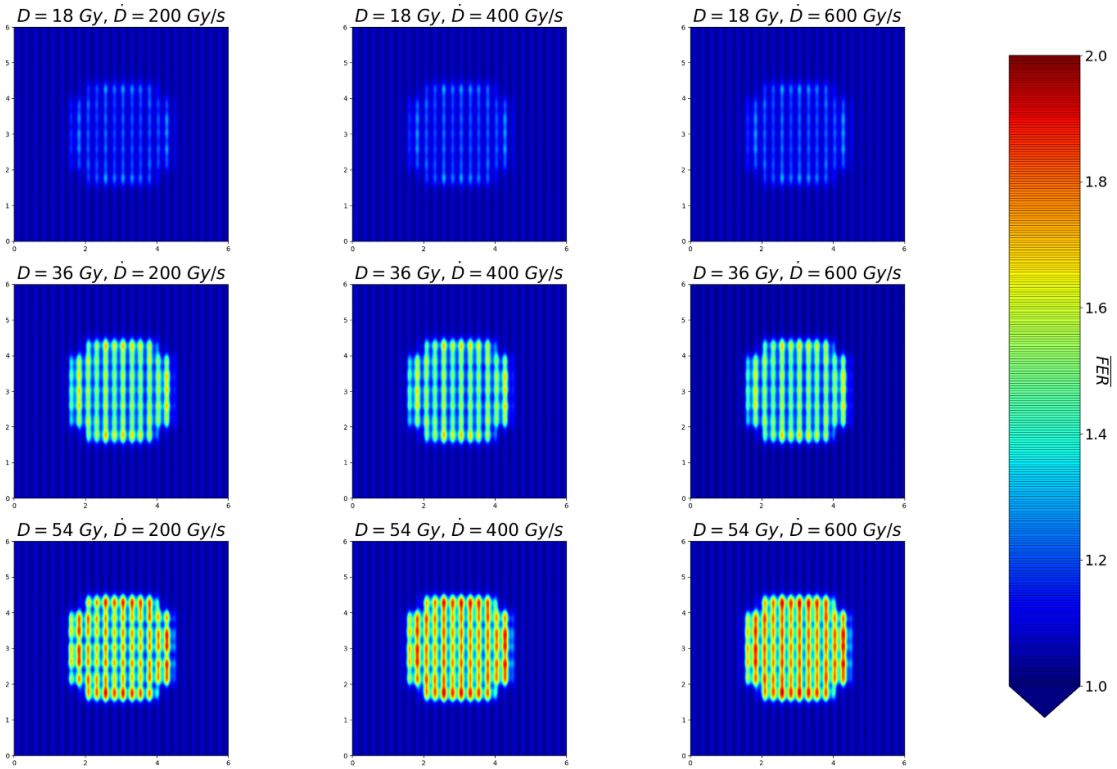

Figure 5. The $\overline{\text{FER}}$ distribution for a dose of $D = [18, 36, 54]$ Gy and a dose rate of $\dot{D} = [200, 400, 600]$ Gy $\cdot$ s^{-1} using a diffusion coefficient of $\mathcal{D} = 1.5 \cdot 10^{-9}$ m$^2 \cdot$ s^{-1}. The low steady-state for a diffusion coefficient of $\mathcal{D} = 1.5 \cdot 10^{-9}$ m$^2 \cdot$ s^{-1} results in an immediate FLASH effect throughout a large part of the tissue.

$\mathcal{D} = 1.5 \cdot 10^{-9}$ m$^2 \cdot$ s^{-1} of the diffusion coefficient, the system is already hypoxic in steady state. This results in a small but observable FLASH effect outside the PTV.

Comparing figure 5 with figure 6 illustrates the impact of a larger diffusion coefficient on the impact of the FLASH effect through a lack of oxygen enhancement. For $\mathcal{D} = 2.0 \cdot 10^{-9}$ m$^2 \cdot$ s^{-1} and $D = 18$ Gy, the

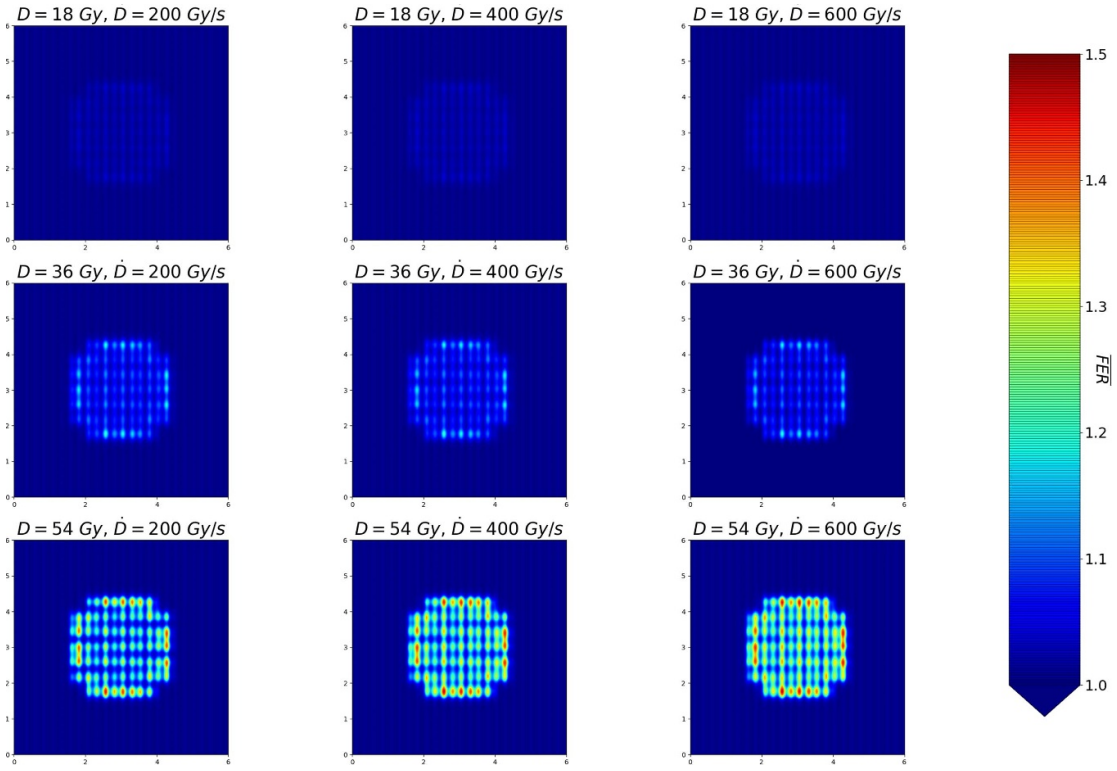

Figure 6. The $\overline{\text{FER}}$ distribution for a dose of $D = [18, 36, 54]$ Gy and a dose rate of $\dot{D} = [200, 400, 600]$ Gy $\cdot$ s^{-1} using a diffusion coefficient of $\mathcal{D} = 2.0 \cdot 10^{-9}$ m^2 $\cdot$ s^{-1}. Note the difference in colour-bar range when compared to figure 5.

FLASH effect is small, at $D = 36$ Gy the effect is significant only near the centre of the pencil beams, while for $\mathcal{D} = 1.5 \cdot 10^{-9}$ m^2 $\cdot$ s^{-1} the FLASH effect is always significant, even at the lowest dose and DR.

In both cases, the FLASH effect increases with increasing dose (from top to bottom) and DR (from left to right). At typical scales of dose and DR, as studied here, the impact of DR is smaller than that of dose, especially with a lower dose and the larger diffusion coefficient. This is due to the threshold in dose and DR, first the cells have to be irradiated into a hypoxic state, only after which the FLASH effect may be achieved, causing the increase in DR to have larger effect on FLASH at a higher dose and a lower diffusion coefficient. Mainly because a lower diffusion coefficient results in a lower oxygen concentration in steady-state.

3.4. Impact of the scan pattern

Figure 7 displays the distribution of the PBS-DR for the various patterns. The scan pattern has a significant impact on the distribution of the PBS-DR and on the maximal amount achieved. The PBS-DR as a DR metric, proposed by Folkerts *et al* (2020), quantifies local DR variations and the 'snowflake 'pattern is optimised on the PBS-DR in a previous work by José Santo *et al* (2022). The pattern favours pencil-beams which are located close together. Based on the oxygen depletion hypothesis, this should result in lower oxygen concentrations during irradiation and therefore, a larger oxygen induced FLASH effect.

Volume histograms of the FED and the PBS-DR at a constant instantaneous DR of 400 Gy $\cdot$ s^{-1} are displayed in figure 8 for different doses, diffusion coefficients and scan patterns. Furthermore, the dose is displayed when applicable with a solid line.

In figure 8(a) the diffusion coefficient is varied, while the dose and DR are fixed. We observe a small increase in the difference in FLASH impact of the different patterns for a larger diffusion coefficient. The 'snowflake' pattern induces the largest FLASH effect, the 'snake' has a slightly larger FLASH effect than the 'z' pattern. This difference is small but observable for every diffusion coefficient displayed.

In figure 8(b) dose is varied, while the diffusion coefficient and DR are fixed. The lower two doses have no observable difference in FLASH between the patterns. For a dose of $D = 54$ Gy there is a slight difference, where again the 'snowflake' pattern induces the largest FLASH effect, then the 'snake' pattern and then the 'z' pattern.

Figure 8 displays a volume histogram after significantly increasing the dose and the diffusion coefficient. In figures (a) and (b) it is observed that larger diffusion coefficient and dose resulted in a larger difference in patterns. Going to the outer ranges of our parameter regime resulted in a clear distinction between patterns on FLASH. Still the difference in effect is small.

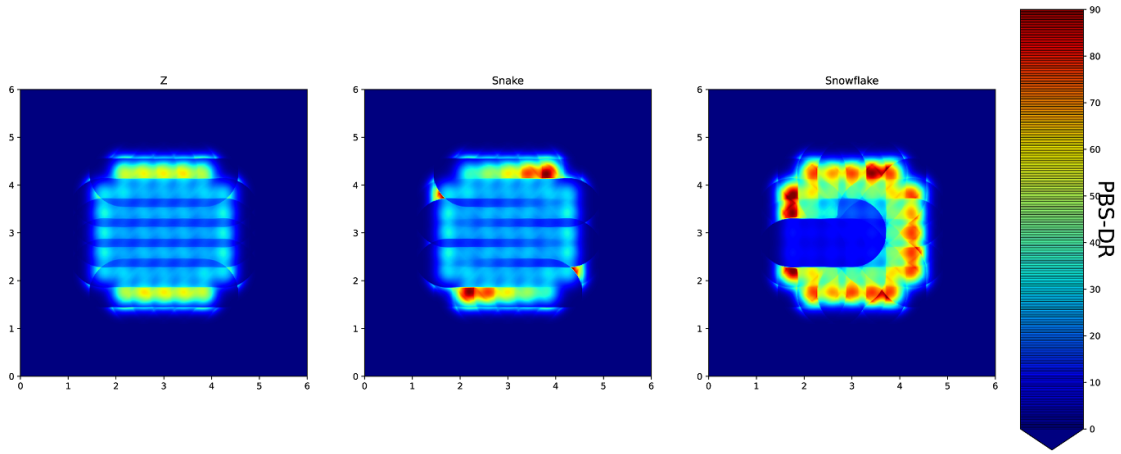

Figure 7. The PBS-DR for the z (left), snake (middle), and snowflake (right) pattern using a dose of $D = 54$ Gy and a dose rate of $\dot{D} = 400\ \mathrm{Gy} \cdot \mathrm{s}^{-1}$.

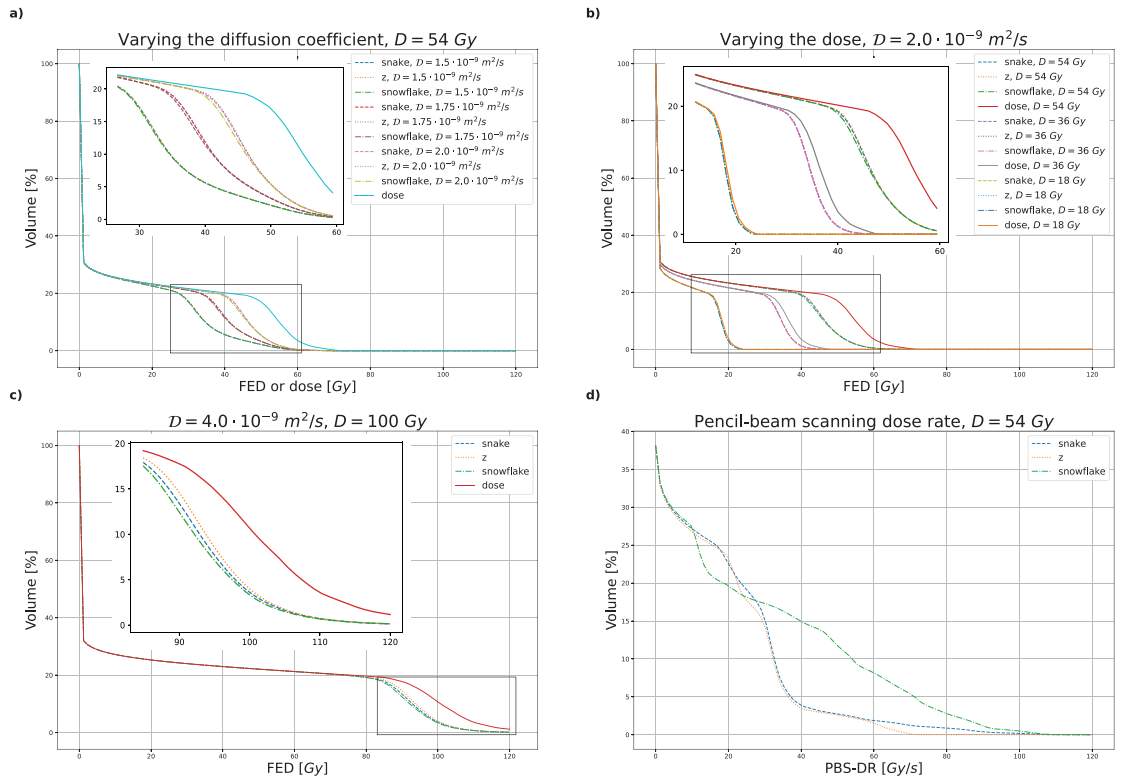

Figure 8. Volume histograms of the FED (a)–(c) for the different doses, diffusion coefficients and patterns, and of the PBS-DR (d) at a fixed dose rate of $\dot{D} = 400\ \mathrm{Gy} \cdot \mathrm{s}^{-1}$. In figure a, b, and c the dose is presented with a solid line. (a) Volume histogram for a diffusion coefficient of $\mathcal{D} = [1.5, 1.75, 2.0] \cdot 10^{-9}\ \mathrm{m}^2 \cdot \mathrm{s}^{-1}$, while keeping the dose fixed at $D = 54$ Gy. (b) Volume histogram for a dose of $D = [18, 36, 54]$ Gy, while keeping the diffusion coefficient fixed at $\mathcal{D} = 2.0 \cdot 10^{-9}\ \mathrm{m}^2 \cdot \mathrm{s}^{-1}$. (c) Volume histogram after increasing the diffusion coefficient to $\mathcal{D} = 4.0 \cdot 10^{-9}\ \mathrm{m}^2 \cdot \mathrm{s}^{-1}$ and the dose to $D = 100$ Gy. (d) Volume histogram for the PBS-DR at a fixed dose of $D = 54$ Gy.

Figure 8(d) displays a volume histogram of the PBS-DR. The different patterns result in large differences in the PBS-DR. The 'snowflake' pattern, optimised on the PBS-DR, induces a significantly larger FLASH effect than the 'snake' and 'z' pattern. The 'snake' pattern has a slightly larger FLASH effect than the 'z' pattern.

3.5. Dependence on dimensionless parameters

Figure 9 displays a three-dimensional scatter plot of the $< \overline{FER} >$ for different parameter configurations. Along the axis are the dimensionless parameter, one of which relates to the diffusion coefficient (horizontal in plane), one to dose (perpendicular to the plane) and one to DR (vertical in plane).

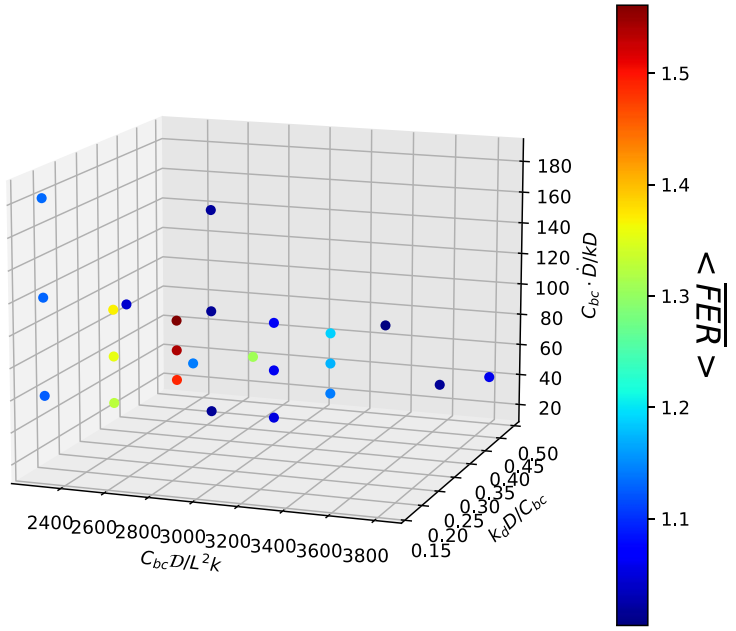

Figure 9. A three-dimensional scatter plot of the $< \overline{\text{FER}} >$ (color scale) for different parameter combinations of the dimensionless model parameters. The axis display dimensionless parameters, where one relates to the diffusion coefficient, one to dose and one to dose rate. For reference the numeric values are displayed in a table in the appendix.

With increasing DR the FLASH effect increases slightly at lower diffusion coefficients and larger doses. For other parameter combinations, this is not observed. Increasing the dose has a significant effect on the magnitude of the FLASH effect, as it leads to a significant increase in FLASH for all parameter combinations explored. This effect is larger at lower diffusion coefficients. Lowering the diffusion coefficient results in a large increase of the magnitude of the FLASH effect, at large diffusion coefficients the FLASH effect is small or not at all observable.

4. Discussion

We have implemented and solved a physical 2D oxygen diffusion model to study the impact of dose delivery in IMPT with PBS and tissue and model parameters on radiolytic depletion and diffusion of oxygen and changes in radiosensitivity through oxygen enhancement. This effect is generally assumed to play an important role in the FLASH effect as observed in preclinical studies (Favaudon 2014, Vozenin *et al* 2019). In this section, we discuss the impact of model parameters and PBS and some limitations of our model.

4.1. Impact of the steady-state and the diffusion coefficient

The steady-state oxygen concentration depends on metabolic oxygen consumption and on diffusion from the capillaries into the tissue. The FLASH effect is determined by the steady-state oxygen concentration, re-oxygenation, dose and DR. For our model, and the (typical) model parameter ranges we have explored, the steady-state oxygen concentration has by far the largest impact on the effective time-averaged FLASH enhancement ratio ($\overline{\text{FER}}$).

Figures 5 and 6 display the difference in $\overline{\text{FER}}$ for a diffusion coefficients of $\mathcal{D} = [1.5, 2.0] \cdot 10^{-9}$ m$^2 \cdot$ s^{-1}. This illustrates the critical dependence of the diffusion and the resulting steady-state oxygen concentration on the $\overline{\text{FER}}$. The larger the oxygen diffusion constant, the higher the steady-state oxygen concentration and the longer it takes to (locally) deplete a substantial amount of oxygen to drive the system into a hypoxic state in which the radiosensitivity is reduced. More diffusion results in a smaller local and global FLASH effect, where the FLASH effect is averaged over delivery time and space through the calculation of dose-volume parameters. This is also clearly visible in figure 9, looking along the diffusion axis, the FLASH effect increases significantly while other parameters are kept constant.

Total dose may also significantly impact the FLASH effect, but only for smaller diffusion coefficients this effect becomes significant. FLASH has a dose threshold before it starts to occur, the diffusion coefficient greatly impacts the steady state and therefore the FLASH dose threshold. Increasing the DR also does have some effect on the amount of FLASH. However, for the (typical) range of doses and DRs analysed here, the effect is significantly smaller than the effect of dose and diffusion.

The relative importance of the diffusion coefficients is expected to be even more prominent in 3D than in 2D, due to the additional spatial direction in which oxygen may (or may not) diffuse. The mean squared displacement of a diffusing particle is proportional to the number of independent degrees of freedom and the diffusion constant (Luzhansky *et al* 2018). Therefore, there could be limitations to the 2D assumption. However, since our use case simulates shoot-through or transmissions beams the difference in dose deposition and hence in the radiolytic depletion along the axis perpendicular to the plane is essentially constant. For diffusion there can be a significant difference between two-and three-dimensions. However, since we model the capillaries on a rectangular grid, if the blood flow is sufficiently large the difference in oxygen levels along the axis perpendicular to the plane in which the capillaries extent becomes small.

Radiolytic depletion is orders of magnitude faster than re-oxygenation making the steady-state an important contributor to the amount of FLASH. The diffusion coefficient is critical for the steady-state, the impact of the diffusion coefficient on re-oxygenation is of less importance since it is much slower. Only for substantially larger irradiated volumes, the time-scale of re-oxygenation and, hence, its impact on the FLASH effect through radiolytic depletion of oxygen may become significant.

The quantitative analysis of the various physiologically realistic model parameters resulted in a lower FLASH effect then previous empirical findings. This indicates that, while oxygen enhancement may be an important contributor to the FLASH effect, oxygen depletion alone may not be sufficient to fully explain the FLASH effect. This is exemplified by the fact that the FLASH effect in our model, resulting from oxygen enhancement, does not quantitatively agree with previous findings in pre-clinical experiments. Figure 6 shows a local $\overline{\text{FER}} \approx 1.5$ at beam locations for a dose of 54 Gy, while in animal experiments, e.g. the study by Favaudon *et al*, results consistent with FLASH enhancement ratios larger than 1.8 at much lower (fraction) doses are reported. However, the actual oxygen concentrations in these experiments are not known. Theoretically, it may be possible to find a combination of parameters for which the steady-state results in a $\overline{\text{FER}}$ which corresponds with phenomenological data. Recently Poulsen *et al* (2023) demonstrated the possibility of finding a local phenomenological oxygen-diffusion based FLASH model (Petersson *et al* 2020) with not-necessarily physiologically realistic model parameters that does correspond with experimental data.

4.2. Impact of patterns

The different delivery patterns taken into account here resulted in small differences in FLASH based on the volume histogram of the FED. The 'snowflake' pattern optimised on the PBS-DR had the largest FLASH effect, the line by line back-and-forth 'snake' pattern resulted in a small increase in FLASH compared to the standard line-by-line 'z' pattern. The 'z' and 'snake' pattern are alike, except for the edge alterations as illustrated in figure 2. The 'snake' pattern has consecutive pencil beams close together on the edges, resulting in a slightly larger FLASH effect in some use-cases. The 'snowflake' pattern is optimised on the PBS-DR. The PBS-DR increases for shorter irradiation time, favouring consecutive beams close to each other. The 'snowflake' pattern results in the largest $\overline{\text{FER}}$. Although quantitatively the PBS-DR and $\overline{\text{FER}}$ do not agree on the impact of various patterns, there is a qualitative agreement between the oxygen diffusion model and the PBS-DR.

The observation that scan-pattern optimisation on the PBS-DR has little impact on the resulting distribution of FED is consistent with our finding that, in our model with the physiologically realistic parameters we investigated, the magnitude of the FLASH effect is dominantly determined by oxygen diffusion and to a much lesser extent by DR. This may be different for larger irradiated volumes, where the time intervals between re-irradiation of the same tissue and hence the impact of re-oxygenation and scan pattern is expected to be more pronounced.

The FLASH effect has a temporal dependence on the pencil-beam distribution due to the thresholds in dose and DR. Due to this temporal dependency, the order in which pencil beams irradiate can be optimised. The threshold effect and the set-off time before the tissue is in a hypoxic state, as well as the saturation effect of FLASH, can be modelled using an oxygen diffusion model. Our oxygen diffusion model predicts small differences between patterns, presumably due to the fast depletion of oxygen and slower re-oxygenation. A pattern optimised on this model may further enhance the FLASH effect. However, when going to more extreme parameter regimes the difference between patterns arguably becomes even smaller. For a hypoxic environment the overall FLASH effect goes to zero as the system is already deep into the FLASH regime and there is always the maximum amount of FLASH. The largest difference in pattern happens when the steady-state is just outside the FLASH regime, which is within the parameter regime we have expored here. The optimised pattern we have tested is optimised on the PBS-DR, which favours consecutive delivery of nearby pencil beams. A pattern optimised on this oxygen-diffusion model would also favour pencil beams which are close together, although the improvement would most probably be small for the field sizes and model parameters studied here.

5. Conclusion

In this paper, we have studied an oxygen-diffusion model to study the FLASH effect in UHDR-PT with PBS, in which the FLASH effect was modeled as the influence of oxygen depletion on the OER. Our main findings are that: (i) the diffusive properties of oxygen in the tissue are critical for the steady-state oxygen concentration and, hence for the FLASH effect. As oxygen depletion is an inverse saturation effect, in which a substantial amount of oxygen needs to be depleted to achieve a sizable reduction of radiosensitivity, and re-oxygenation through diffusion is a slow process, for the UHDR delivery and the model parameters studied here, at fixed oxygen diffusion, (ii) the FLASH effect through oxygen depletion primarily depends on dose. This is exemplified by the results in figures 5 and 6. At a fixed fraction dose, we also observed (iii) a slight dependence on DR, as can be seen in the same figures. As a result, (iv) scan patterns optimised on DR, also perform (slightly) better on our biological model. The results confirm our previous finding that the FLASH effect (may) depend on scan pattern and, hence, that scan pattern in IMPT with PBS can be optimised.

However, for the model parameters and irradiated volumes considered here, and the resulting time intervals between reirradiation of the same tissue, the impact of re-oxygenation through diffusion and that of the PBS-DR and the delivery patterns and the optimisation thereof is small. This may be different for significantly larger irradiated volumes.

The magnitude of the FLASH effect as modeled through radiolytic depletion and diffusion of oxygen, and the threshold values for dose and DR do not quantitatively agree with the observed FLASH effect. A better understanding of the mechanisms underlying the FLASH effect is essential for the further development of FLASH radiotherapy.

Data availability statement

The data cannot be made publicly available upon publication because they are not available in a format that is sufficiently accessible or reusable by other researchers. The data that support the findings of this study are available upon reasonable request from the authors.

Acknowledgment

We thank Krista van Doorn-Wink, MD, PhD for critical reading of the manuscript.

Appendix

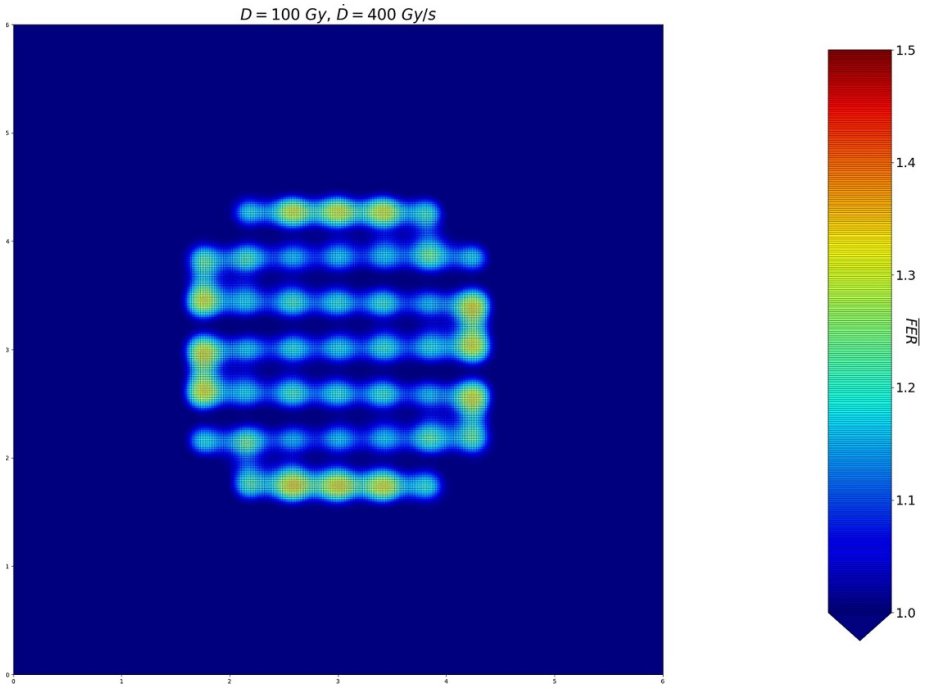

Figure 10. The $\overline{\text{FER}}$ distribution for a dose of $D = 100$ Gy and a dose rate of $\dot{D} = 400$ Gy $\cdot$ s^{-1} using a diffusion coefficient of $\mathcal{D} = 4.0 \cdot 10^{-9}$ m^2 $\cdot$ s^{-1}.

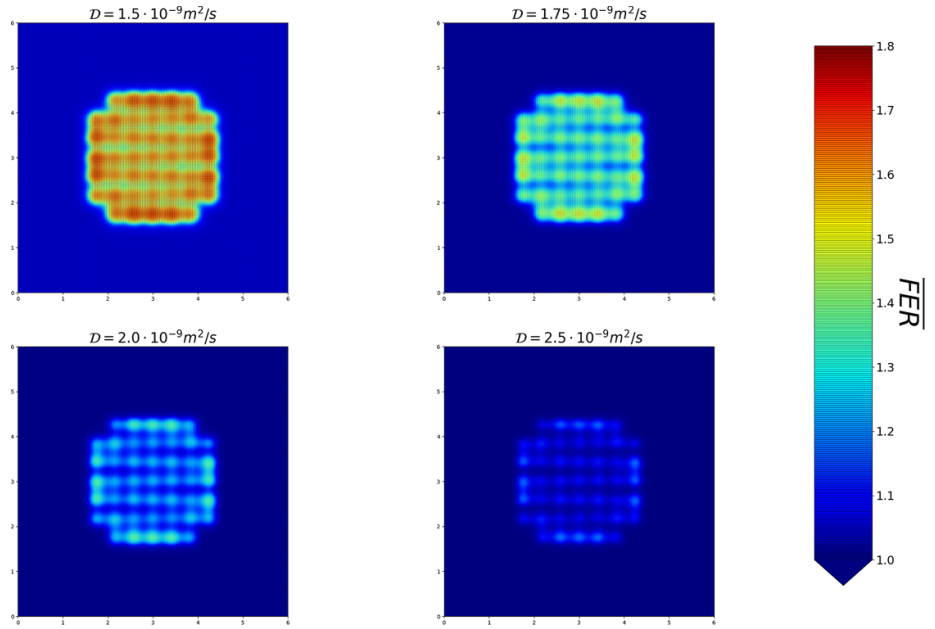

Figure 11. The $\overline{\text{FER}}$ distribution for a dose of $D = 54$ Gy and a dose rate of $\dot{D} = 400$ Gy $\cdot$ s^{-1} using a diffusion coefficient of $\mathcal{D} = [1.5, 1.75, 2.0, 2.5] \cdot 10^{-9}$ m$^2 \cdot$ s^{-1}.

Table 2. table with input values for the three-dimensional plot in figure 9.

Diffusion coefficient [m$^2 \cdot$ s^{-1}]	Dose [Gy]	Dose rate [Gy/s]	Pattern	$< \overline{\text{FER}} >_{\text{PTV}}$
2,5	18	400	Snake	1.0041
2,5	36	400	Snake	1.0159
2	18	400	Snake	1.0171
1,75	18	400	Snake	1.0418
2,5	54	400	Snake	1.0567
2	36	400	Snake	1.0590
1,5	18	400	Snake	1.1302
1,75	36	400	Snake	1.1423
2	54	400	Snake	1.1730
1,75	54	400	Snake	1.3079
1,5	36	400	Snake	1.3564
1,5	54	400	Snake	1.5391
1,5	18	200	Snake	1.1259
1,5	18	600	Snake	1.1316
1,5	36	200	Snake	1.3259
1,5	36	600	Snake	1.3689
1,5	54	200	Snake	1.4873
1,5	54	600	Snake	1.5610
2	18	200	Snake	1.0166
2	18	600	Snake	1.0173
2	36	200	Snake	1.0518
2	36	600	Snake	1.0622
2	54	200	Snake	1.1419
2	54	600	Snake	1.1882

References

Adrian G, Konradsson E, Lempart M, Bäck S, Ceberg C and Petersson K 2020 The flash effect depends on oxygen concentration *Br. J. Radiol.* **92** 20190702

Almeida A *et al* 2024 Antitumor effect by either flash or conventional dose rate irradiation involves equivalent immune responses *Int. J. Radiat. Oncol. Biol. Phys.* **118** 1110–22

Berry R J, Hall E J, Forster D W, Storr T H and Goodman M J 1969 Survival of mammalian cells exposed to x rays at ultra-high dose-rates *Br. J. Radiol.* **42** 102–7

Bourhis J, Jeanneret Sozzi W, Gonçalves Jorge P, Gaide O, Bailat C, Duclos F, Patin D, Ozsahin M, Bochud F and Germond J-F 2019 Treatment of a first patient with flash-radiotherapy *Radiother. Oncol.* **139** 18–22

Mascia A E 2023 Proton FLASH Radiotherapy for the Treatment of Symptomatic Bone Metastases: The FAST-01 Nonrandomized Trial *JAMA Oncol.* **9** 62
Chappuis F, Ngoc Tran H, Zein S A, Bailat C, Incerti S, Bochud F and Desorgher L 2023 The general-purpose geant4 monte carlo toolkit and its geant4-dna extension to investigate mechanisms underlying the flash effect in radiotherapy: current status and challenges *Phys. Med.* **110** 102601
Clark D S and Blanch H W 1997 *Biochemical Engineering* (CRC Press)
Deffet S and Sterpin E 2023 Optimization of pencil beam scanning pattern for flash proton therapy (https://doi.org/https://doi.org/10.48550/arXiv.2304.05721)
Delft High Performance Computing Centre (DHPC) 2022 DelftBlue Supercomputer (Phase 1) (available at: www.tudelft.nl/dhpc/ark:/44463/DelftBluePhase1)
Dewey D L and Boag J W 1959 Modification of the oxygen effect when bacteria are given large pulses of radiation *Nature* **183** 1450–1
Favaudon V *et al* 2014 Ultrahigh dose-rate flash irradiation increases the differential response between normal and tumor tissue in mice *Sci. Trans. Med.* **6** 245ra93
Folkerts M M, Abel E, Busold S, Rika Perez J, Krishnamurthi V and Clifton Ling C 2020 A framework for defining flash dose rate for pencil beam scanning *Med. Phys.* **47** 6396–404
Germer T, Uelwer T, Conrad S and Harmeling S 2020 Pymatting: a python library for alpha matting *J. Open Source Softw.* **5** 2481
Habraken S, Breedveld S, Groen J, Nuyttens J and Hoogeman M 2022 Trade-off in healthy tissue sparing of flash and fractionation in stereotactic proton therapy of lung lesions with transmission beams *Radiother. Oncol.* **175** 231–7
Hornsey S and Alper T 1966 Unexpected dose-rate effect in the killing of mice by radiation *Nature* **210** 212–3
Hornsey S and Bewley D K 1971 Hypoxia in mouse intestine induced by electron irradiation at high dose-rates *Int. J. Radiation Biol. Related Stud. Phys., Chem. Med.* **19** 479–83
Hu A, Qiu R, Wu Z, Zhang H, Bo Li W B and Junli J 2022 A computational model for oxygen depletion hypothesis in flash effect *Radiat. Res.* **197** 175–83
Hughes J R and Parsons J L 2020 Flash radiotherapy: current knowledge and future insights using proton-beam therapy *Int. J. Mol. Sci.* **21** 6492
Jin J-Y, Anxin G, Wang W, Oleinick N L, Machtay M and (Spring) Kong F-M 2020 Ultra-high dose rate effect on circulating immune cells: A potential mechanism for flash effect? *Radiother. Oncol.* **149** 55–62
José Santo R, Habraken S J M, Breedveld S and Hoogeman M S 2022 Pencil-beam delivery pattern optimization increases dose rate for stereotactic flash proton therapy *Int. J. Radiat. Oncol. Biol. Phys.* **115** 759–67
Krieger M, van de Water S, Folkerts M M, Mazal A, Fabiano S, Bizzocchi N, Weber D C, Safai S and Lomax A J 2022 A quantitative flash effectiveness model to reveal potentials and pitfalls of high dose rate proton therapy *Med. Phys.* **49** 2026–38
Levy K *et al* 2020 Abdominal flash irradiation reduces radiation-induced gastrointestinal toxicity for the treatment of ovarian cancer in mice *Sci. Rep.* **10** 1–14
Luzhansky I D, Schwartz A D, Cohen J D, MacMunn J P, Barney L E Jansen L E and Peyton S R 2018 Anomalously diffusing and persistently migrating cells in 2D and 3D culture environments *APL Bioeng.* **2** 266112
Michaelis L and Menten M L 2013 The kinetics of invertin action *FEBS Lett.* **587** 2712–20
Montay-Gruel P *et al* 2019 Long-term neurocognitive benefits of flash radiotherapy driven by reduced reactive oxygen species *Proc. Natl Acad. Sci.* **116** 10943–51
Montay-Gruel P *et al* 2021 Hypofractionated flash-rt as an effective treatment against glioblastoma that reduces neurocognitive side effects in mice *Clin. Cancer Res.* **27** 775–84
Morgan W F and Sowa M B 2005 Effects of ionizing radiation in nonirradiated cells *Proc. Natl Acad. Sci.* **102** 14127–8
Paganetti H, Niemierko A, Ancukiewicz M, Gerweck L E, Goitein M, Loeffler J S and Suit H D 2002 Relative biological effectiveness (rbe) values for proton beam therapy *Int. J. Radiat. Oncol. Biol. Phys.* **53** 407–21
Petersson K, Adrian G, Butterworth K and McMahon S J 2020 A quantitative analysis of the role of oxygen tension in flash radiation therapy *Int. J. Radiat. Oncol. Biol. Phys.* **107** 539–47
Poulsen P, Kanouta E, Sitarz M, Johansen J, Andersen C Grau C and Sørensen B 2023 Mo-0720 proton flash: Impact of dose rate on biological response in an acute damage mouse model *Radiother. Oncol.* **182** S589–90
Pratx G and Kapp D S 2019 A computational model of radiolytic oxygen depletion during flash irradiation and its effect on the oxygen enhancement ratio *Phys. Med. Biol.* **64** 185005
Puthenparampil Wilson B J, Yokoi T, Hill M and Vojnovic B 2012 Revisiting the ultra-high dose rate effect: implications for charged particle radiotherapy using protons and light ions *Br. J. Radiol.* **85** e933–9
Robert Grimes D and Partridge M 2015 A mechanistic investigation of the oxygen fixation hypothesis and oxygen enhancement ratio *Biomed. Phys. Eng. Express* **1** 045209
Rothwell B C, Kirkby N F, Merchant M J, Chadwick A L, Lowe M, Mackay R I, Hendry J H and Kirkby K J 2021 Determining the parameter space for effective oxygen depletion for flash radiation therapy *Phys. Med. Biol.* **66** 055020
Schüler E, Eriksson K, Hynning E, Hancock S L, Hiniker S M, Bazalova-Carter M, Wong T, Quynh-Thu L, Loo B W and Maxim P G 2017 Very high-energy electron (vhee) beams in radiation therapy; treatment plan comparison between vhee, vmat and ppbs *Med. Phys.* **44** 2544–55
Secomb T W, Hsu R, Dewhirst M W, Klitzman B and Gross J F 1993 Analysis of oxygen transport to tumor tissue by microvascular networks *Int. J. Radiat. Oncol. Biol. Phys.* **25** 481–9
Spitz D R, Buettner G R, Petronek M S, St-Aubin J J, Flynn R T, Waldron T J and Limoli C L 2019 An integrated physico-chemical approach for explaining the differential impact of flash versus conventional dose rate irradiation on cancer and normal tissue responses *Radiother. Oncol.* **139** 23–27
Town C D 1967 Effect of high dose rates on survival of mammalian cells *Nature* **215** 847–8
van Marlen P, Dahele M Folkerts M M, Slotman B J and Verbakel W F A R 2020 Conventionally fractionated flash treatment planning for head and neck cancer using transmission beam proton therapy *Int. J. Radiat. Oncol. Biol. Phys.* **108** S186–7
Vozenin M-C, Bourhis J and Durante M 2022 Towards clinical translation of flash radiotherapy *Nat. Rev. Clin. Oncol.* **19** 791–803
Vozenin M-C, De Fornel P, Petersson K, Favaudon V, Jaccard M, Germond J-F, Petit B, Burki M, Ferrand G'ele and Patin D 2019 The advantage of flash radiotherapy confirmed in mini-pig and cat-cancer patients - the advantage of flash radiotherapy *Clin. Cancer Res.* **25** 35–42

Wardman P 2020 Radiotherapy using high-intensity pulsed radiation beams (flash): a radiation-chemical perspective *Radiat. Res.* **194** 607–17

Weiss H, Epp E R, Heslin J M, Ling C C and Santomasso A 1974 Oxygen depletion in cells irradiated at ultra-high dose-rates and at conventional dose-rates *Int. J. Radiat. Biol. Related Stud. Phys., Chem. Med.* **26** 17–29

Zhu H, Junli Li, Deng X, Qiu R, Zhen W and Zhang H 2021 Modeling of cellular response after flash irradiation: a quantitative analysis based on the radiolytic oxygen depletion hypothesis *Phys. Med. Biol.* **66** 185009